Polym. Bull. (2011) 67:885–902
DOI 10.1007/s00289-011-0518-8

ORIGINAL PAPER

Morphologies and structures in poly(L-lactide-*b*-ethylene oxide) copolymers determined by crystallization, microphase separation, and vitrification

Shaoyong Huang · Hongfei Li · Shichun Jiang · Xuesi Chen · Lijia An

Received: 20 February 2011 / Revised: 16 May 2011 / Accepted: 22 May 2011 /
Published online: 3 June 2011

Abstract Morphologies and structures determined by crystallization of the blocks, microphase separation of the copolymers, and vitrification of PLLA block in poly(L-lactide-*b*-ethylene oxide) (PLLA-*b*-PEO) copolymers were investigated using microscopic techniques and synchrotron small angle X-ray scattering. The PLLA-*b*-PEO copolymer films were crystallized from two different annealing processes: melt crystallization (process A) or crystallized from glass state of PLLA block after quenching from melt state (process B). The relationship between the crystalline morphology and microstructure of the copolymers were explored using SAXS. The morphology and phase structure are predominated by crystallization of PLLA block, and greatly influenced by microphase separation of the copolymers. In process B, lozenge-shape and truncated lozenge-shaped PLLA crystals of nanometer scale can be observed. The crystalline morphology is markedly affected by the microstructure formed during the annealing process. Star-shaped morphologies stacked with PLLA single crystals were observed.

Keywords Crystallization · Morphology · Structure · Microphase separation · Vitrification · Poly(L-lactide-*b*-ethylene oxide) copolymer

S. Huang · H. Li · L. An (✉)
State Key Laboratory of Polymer Physics and Chemistry, Changchun Institute of Applied Chemistry, Chinese Academy of Sciences, Changchun 130022, People's Republic of China
e-mail: ljan@ciac.jl.cn

S. Huang · X. Chen
Key Laboratory of Polymer Ecomaterials, Changchun Institute of Applied Chemistry, Chinese Academy of Sciences, Changchun 130022, People's Republic of China

S. Jiang (✉)
School of Materials Science and Engineering, Tianjin University, Tianjin 300072, People's Republic of China
e-mail: scjiang@tju.edu.cn

Introduction

During the past several decades, extensive research related to diblock copolymers has been carried out. Diblock copolymers are an interesting option, where combinations of different chemical structures employed without macroscopic phase separation [1]. The ability of block copolymers to self-assemble in the melt according to the relative thermodynamic repulsion between their components is well known and has been extensively investigated theoretically and experimentally [1–5]. For amorphous diblock copolymers, microphase separation is driven by the immiscibility between the block copolymer components. Ordered morphologies can be observed when the glass transition temperatures (T_g) of the two phase-separated components are lower than the order-to-disorder transition temperature (T_{ODT}) [6]. However, crystalline–amorphous diblock copolymers possess more complicated phase behavior due to the crystallization of the crystallizable component. When the T_g of the miscible copolymer is lower than the crystallization temperature of the crystallizable component quenched from the melt, the final microphase separation is actually driven by the crystallization of this component, and a lamellar morphology, in which the lamellar crystals are sandwiched by the amorphous-block layers, is always observed after crystallization. In an immiscible crystalline–amorphous diblock copolymer system, it can be expected that self-organization of the diblock copolymer, vitrification of the amorphous block, and crystallization of the crystallizable block may compete with one another in forming the final morphologies at different temperatures. Three temperature parameters need to be considered to describe the competitions: the T_{ODT}, the T_g of the amorphous phase, and the T_c. Depending on segregation strength and the relative location of T_{ODT}, T_g and T_c, different morphologies can be generated. Either crystallization can drive structure formation for weakly segregated melt, or crystallization can be confined within the copolymer microdomain structure for strongly segregated systems or homogenous systems. Meanwhile, the competition between microphase separation and crystallization in block copolymers will form abundant morphologies and microstructures [7–12].

Diblock copolymers with one or more biodegradable or/and biocompatible components, which possess promising application in biomedical and environmentally friendly fields, have attracted extensive interest [1, 13–18]. Among biodegradable block copolymers, poly(L-lactide-*b*-ethylene oxide) (PLLA-*b*-PEO) is one of the most important biomaterials, which has been widely investigated on its crystallization and morphological behaviors [15–22]. The two unlike components in PLLA-*b*-PEO copolymers, where the weight fraction of PEO block is above 20 wt%, can both crystallize under right conditions [15, 16, 23]. In contrast, when the weight fraction of PEO block is below 20 wt%, it is difficult for PEO to crystallize [16, 24]. The two blocks are miscible (or partial miscible) at T_m (or T_g) of PLLA block [15, 16, 19, 23–25]. The crystallinity of PLLA is 38–56% when the weight fraction of PLLA is ca. 80 wt% [25].

However, the morphology and structure of PLLA-*b*-PEO copolymers are not fully understood. Especially their morphological behavior and phase structures crystallized from the glass state of PLLA block have never been investigated.

Accordingly, we studied the influence of two different annealing processes on the morphologies and phase structures of PLLA-*b*-PEO diblock copolymers. It is known that the crystallization temperatures (T_c) and the T_gs of PLLA block are higher than the melting points of PEO block in the copolymers [15, 16, 23–25]. During melt crystallization (process A), the PLLA-*b*-PEO copolymers were completely melted at 180 °C, and then cooled to temperatures for crystallization. Microphase separation of the copolymers is driven by crystallization of PLLA block, and the resulting microstructures formed have soft confinement on further crystallization of PLLA block. However, the fractions of PEO block are quite small (<25%) in the copolymers, and the two unlike blocks are miscible in the melt. Consequently, the morphology and structures of the PLLA-*b*-PEO copolymers are predominated by the crystallization of PLLA block. In process B, the copolymer films were quickly cooled to 30 °C after completely melted, which is lower than T_g of PLLA block, kept at 30 °C for 5 min, and then heated to temperatures for isothermal crystallization. In the case of process B, microphase separation of the copolymers is driven by crystallization of PEO block in PLLA16k-*b*-PEO5k copolymer, and maybe including the immiscibility of the two unlike blocks at low temperature, and vitrification of PLLA block takes place under its T_g. The microstructure formed would affect the following crystallization of PLLA block and the structure of the copolymers.

In the present work, the morphologies and structures of the PLLA-*b*-PEO diblock copolymers and PLLA homopolymer determined by the annealing processes were investigated by polarized optical microscope, atomic force microscope, and synchrotron small angle X-ray scattering (SAXS).

Experimental section

Materials

PLLA-*b*-PEO diblock copolymers were synthesized according to the reference [15]. Samples were classified by GPC (Waters 400, USA, software for GPC is Empower with Cirrus™) and purified by a sedimentation method. The copolymers were named as PLLA16k-*b*-PEO5k and PLLA30k-*b*-PEO5k. 16k, 30k, and 5k (g/mol) are the number average molecular weights of each block determined by GPC using PS standard, respectively. PLLA homopolymer used was purchased from Aldrich. The properties including the characteristic temperatures of the copolymers and the homopolymer used are shown in Table 1, which have been reported at reference [16].

Sample preparation

PLLA-*b*-PEO copolymer and PLLA homopolymer films were prepared by coating 0.5% (wt/wt) copolymer–chloroform solutions on clean silicon wafers. After the solvent was completely evaporated, the samples were melted on a Linkam TMS94 hot stage, and then annealed according to process A or B for crystallization. After

Table 1 Characteristic temperature determined by DSC for PLLA-*b*-PEO copolymers, PEO, and PLLA homopolymers used

Sample	Polydispersity (M_w/M_n)	T_g (°)	T_m (°)		T_c (°)	
			PEO	PLLA	PEO	PLLA
PEO5k			61.8		37.3	
PLLA31k	1.39	60.1		170.2		102.4
PLLA16k-*b*-PEO5k	1.40	49.4	41.2	124.4/141.2		90.6
PLLA30k-*b*-PEO5k	1.62	54.3	39.7	142.1		100.0

crystallization, the samples were cooled rapidly to room temperature. The whole processes were carried out in a nitrogen atmosphere.

Polarized optical microscopy

The morphology observations of the PLLA-*b*-PEO copolymers and PLLA homopolymers were performed with a Leica optical microscope (Leica, LM_1-113, Germany), equipped with a hot stage (Linkam TMS94) and a Panasonic CCD camera system.

Atomic force microscopy

The detailed morphologies and microstructures of the samples prepared were observed employing atomic force microscopy (AFM) (Seiko Instruments Inc., SPA300HV with a SPI3800N controller). A 150 μm scanner and SiN_4 cantilevers with spring constant of 42 N/m were applied for tapping mode imaging. Both height and phase images were recorded simultaneously using the retrace signal at room temperature.

Small angle X-ray scattering

The SAXS experiments were performed using synchrotron radiation with $\lambda = 0.156$ nm at Beamline BL15A of Beijing Synchrotron Radiation Facility (Beijing, China). Time-resolved synchrotron SAXS investigations were carried out at the beamlines with heater and a thermal control system (Linkam CSS450). All of the data were corrected for background scattering before analysis and treated with software Fit2D [26]. The structural changes during the heating, annealing, and isothermal processes were followed.

Using software Fit2D, the typical 1D SAXS pattern for crystallized polymer was obtained which is shown in Fig. 1a. Structural parameters including the long period (L), crystal thickness (d_c), amorphous layer thickness (d_a), and transition layer thickness (d_{tr}) can be calculated employing one-dimensional electron density correlation function $K(z)$, where $I(s)$ is the scattering intensity, s denotes the scattering vector $s = 2\sin\theta/\lambda = q/2\pi$.

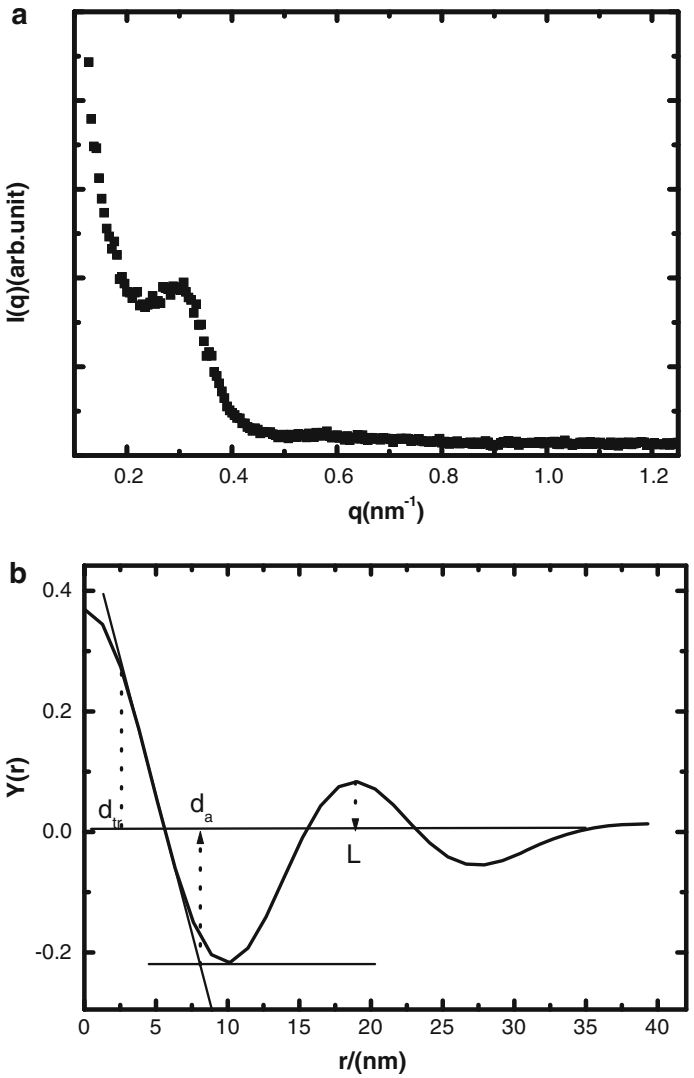

Fig. 1 **a** Typical SAXS pattern for crystallized polymer samples. **b** Structure analysis using one-dimensional electron density correlation function. L, d_a, and d_{tr} means the long period, the amorphous layer thickness, and the transition layer thickness, respectively

$$K(Z) = \frac{1}{2\pi}\int_0^\infty I(s)s^2\cos(sZ)\mathrm{d}s$$

Using $K(z)$ to Fig. 1a, Fig. 1b is received, and then structural parameters are calculated. The relationship between them is $L = d_a + d_c + 2d_{tr}$.

Results and discussion

Morphologies and structures determined by crystallization and microphase separation in melt crystallization

PLLA-*b*-PEO diblock copolymer films were completely melted at 180 °C on a Linkam TMS94 hot stage, and then cooled to T_c for isothermal crystallization. The morphologies observed by polarized optical microscopy (POM) are shown in Fig. 2. Spherulites were observed in the films crystallized at 90 and 100 °C as shown in Fig. 2a and b. Banded spherulites were formed when crystallized at 110 °C from the disordered state shown in Fig. 2c. The spherulitic morphologies of PLLA and its copolymers have been widely reported. An interesting morphology of which the center is spherulite and the outer is dendrite was observed at $T_c = 115$ °C shown in Fig. 2d. When crystallized at higher temperatures, dendrites were formed. Dense dendrites were formed at 120 °C shown in Fig. 2e, the morphology composed of the main branches was star-shaped, and the second branches grew along the main branches. Moreover, the second branches in one side of one main branch were parallel to each other, and the angle between the second branch and the main branch was <90°, which can be ascribed to the influence of the addition of PEO block. At even higher T_c, peculiar dendrites were formed shown in Fig. 2f at 125 °C. The morphologies composed of the main branches were still star-shaped, but the number of the main branch was much smaller than that in dense branches. The angle between the second (third) branch and the main (second) branch was almost 90°. The morphological transition from spherulitic to dendritic in asymmetric PLLA-*b*-PEO copolymers has been first reported in the previous work [16]. Furthermore, in the following, we will try to explore the relationship between the morphology and the microstructure of the copolymers by SAXS technique.

It has been reported that there is a boundary temperature for the PLLA-*b*-PEO copolymers, ca. 115 °C, which divides the crystallization of the copolymers into the low- and the high-crystallization temperature ranges, of which the nucleation, growth rate, and morphology measured at macroscale are distinguished [16, 20–22, 27]. PLLA homopolymer also has a boundary temperature (ca. 120 °C) in terms of the growth rate and crystal structure [28–32], but the crystalline morphologies at various crystallization temperatures are all spherulitic. Comparison with PLLA homopolymer, the addition of PEO block in PLLA-*b*-PEO copolymers, microphase separation and crystallization of the copolymers dominate the morphology and structure.

A synchronous SAXS was employed to explore the structural transition in melt crystallization process. Figure 3a shows the SAXS patterns of PLLA16k-*b*-PEO5k copolymer samples scanned at 120, 110, and 100 °C after crystallization annealed from the melt. Scattering peaks can be seen in the SAXS patterns, indicating that disorder-to-order transition occurs driven by crystallization of PLLA block, which has been confirmed by wide angle X-ray diffraction [15, 16]. The crystallinity of the samples is ca. 30%. The structural parameters including the long period (L), the amorphous layer thickness (d_a), and the transition layer thickness d_{tr}, were received via one-dimensional electron density correlation function, and then the crystal

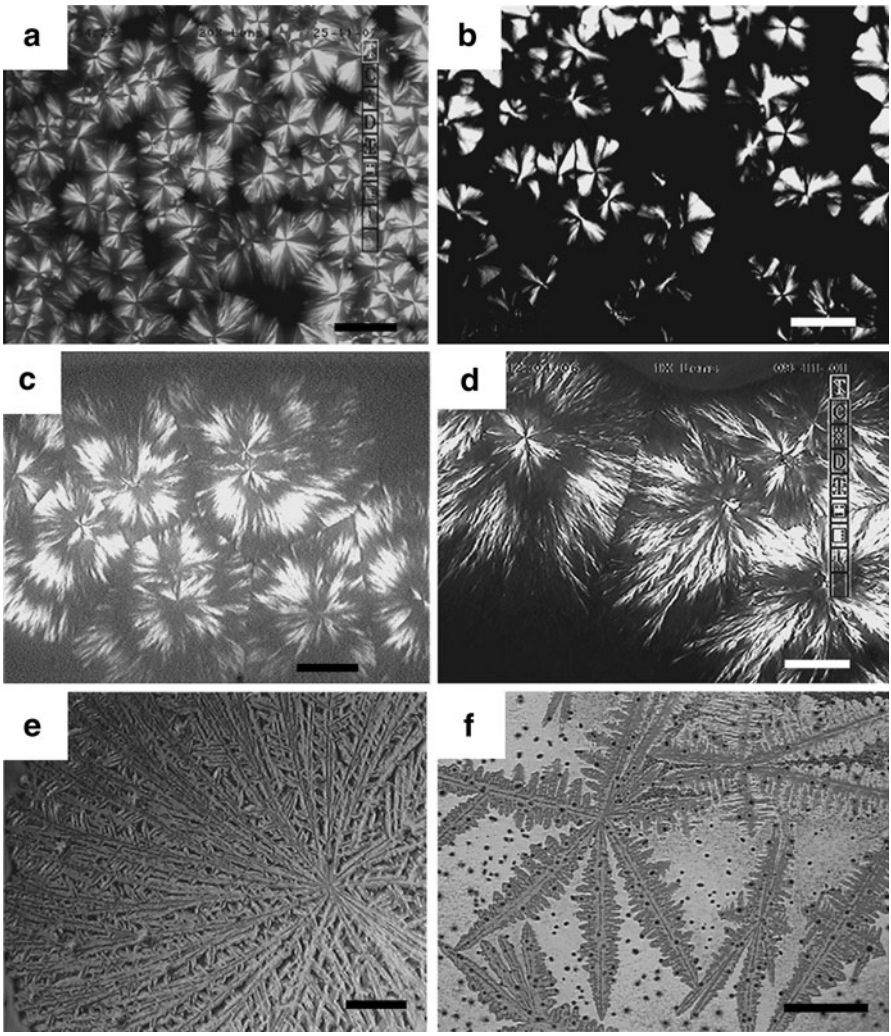

Fig. 2 Morphologies of PLLA16k-*b*-PEO5k copolymer films crystallized at **a** 90, **b** 100, **c** 110, **d** 115, **e** 120, and **f** 125 °C from the melt. The *bar* corresponds to 100 μm

thickness d_c can be calculated using the equation $d_c = L - d_a - 2d_{tr}$. The values of L, d_c, and d_a for PLLA-*b*-PEO copolymer crystallized at 100 °C are 15.0, 4.6, and 7.6 nm, respectively. The values of d_c and d_a increase slightly to 4.7 and 7.6 nm, respectively, at 110 °C. The corresponding crystalline morphologies at 100 and 110 °C are both spherulitic. While for PLLA-*b*-PEO copolymer films crystallized at 120 °C from the melt, the long period increases to 16.3 nm, and the crystal thickness is 4.8 nm, while the amorphous layer thickness is nearly 8.8 nm. The morphology at 120 °C is dense branched, which is different from the morphologies in the low temperature range. At 125 °C shown in Fig. 2f, dendritic morphology was observed.

Fig. 3 **a** SAXS patterns of PLLA16k-*b*-PEO5k copolymer isothermally crystallized at 100, 110, and 120 °C for 15 min from the melt. **b** Structural parameters including L, d_c, and d_a corresponding to (**a**). **c** The morphology changes with microstructure and crystallization temperature

Based on the analysis of the SAXS data, we found that the values of d_a/L calculated from SAXS increase with temperature. In the low-temperature range ($T_c < 115$ °C), the values of d_a/L are ca. 0.50, while in the high-temperature range ($T_c > 115$ °C), the value of d_a/L are ca. 0.54 at 120 °C. Interestingly, the morphology change can be shown as a function of the value of d_a/L in Fig. 3c, indicating the increase of the volume fraction of amorphous phase is probably related to the formation of dendrites at high T_c. T_b defined as the boundary temperature, which classifies the nucleation, morphology, and crystallization of PLLA block into the high- and low-temperature range. It is known that the morphology and structure of PLLA-*b*-PEO copolymers were determined by the interplay of crystallization (nucleation, PLLA chain diffusion, and growth) of PLLA block and the simultaneous microphase separation of PLLA and PEO blocks. In the process, nucleation and crystallization growth of PLLA occurred driven by supercooling. PLLA block can preferentially attach on the growth front around the crystallization growth points. At 100 and 110 °C, the supercooling is relatively large, and then nucleation and crystallization occur quickly. Meanwhile, the volume fraction of amorphous layer is relatively small in the initial stage confirmed by SAXS, indicating the confinement on the PLLA chain diffusion is relatively weak. Spherulitic morphology is produced. At 120 °C, the supercooling is relatively small, and it is difficult for nucleation. PLLA- and PEO-rich domains are formed by microphase separation which is driven by crystallization of PLLA, but the volume fraction of amorphous layer is relatively larger revealed by SAXS. The accumulation of amorphous components in the vicinity of the protrusions of crystallization growth points reduced the super-saturation of PLLA in PLLA-rich domains, and prevents further growth in the immediate vicinity of the trailing edge by confining the diffusion of PLLA chains. Consequently, branched or dendritic morphologies are formed, and the amorphous phases are distributed among the crystalline branches of PLLA. At 115 °C shown in Fig. 2d, the peculiar morphology is the transitional morphology from spherulite to dense branches.

The morphologies of PLLA16k-*b*-PEO5k copolymer films crystallized at low crystallization temperatures (55 and 60 °C) from the melt state were also investigated, they were shown in Fig. 4a and b. Separate spherulites can be obviously observed by POM. For PLLA homopolymer, separate spherulite can only be observed by POM at 80 °C (Fig. 5c) and above (e.g., 88 °C shown in Fig. 5d). Dense small spherulites are formed at 75 °C (Fig. 5a) and 78 °C (Fig. 5b). Comparison the morphologies of PLLA16k-*b*-PEO5k copolymer in Fig. 4 and those of PLLA homopolymer in Fig. 5, the addition of PEO block influences the crystallization behavior of PLLA block, which leads to a decrease in the crystallization temperature of PLLA block, nucleation, and the size of spherulite at low T_c. The morphology and structure of PLLA-*b*-PEO copolymers determined by microphase and separation from the melt were investigated. The results indicated

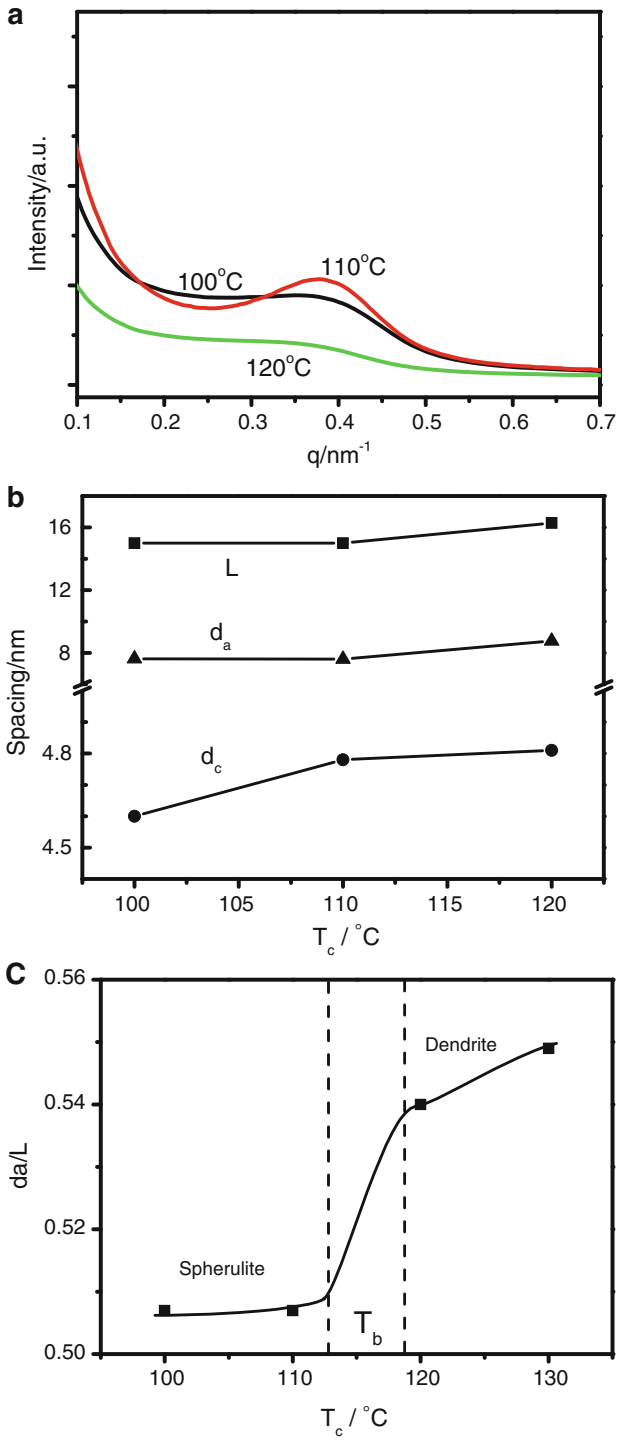
a
Intensity/a.u.
100°C
110°C
120°C
0.1
0.2
0.3
0.4
0.5
0.6
0.7
q/nm-1
b
Spacing/nm
16
12
8
4.8
4.5
L
da
dc
100
105
110
115
120
Tc / °C
C
da/L
0.56
0.54
0.52
0.50
Dendrite
Spherulite
Tb
100
110
120
130
Tc / °C

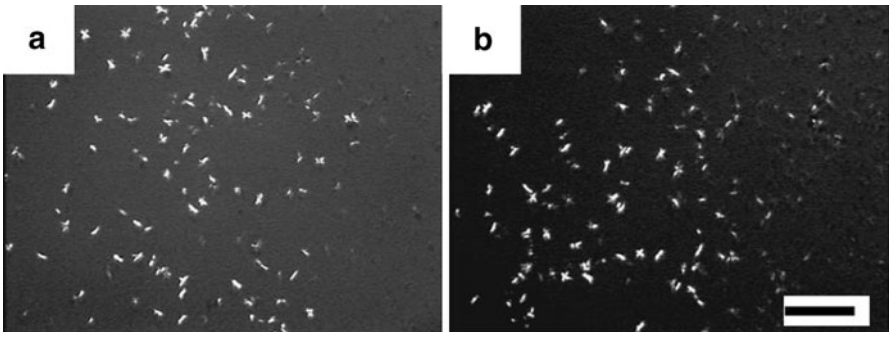

Fig. 4 Morphologies in PLLA16k-*b*-PEO5k copolymer films crystallized at **a** 55 and **b** 60 °C from melt state. The *bar* corresponds to 100 μm

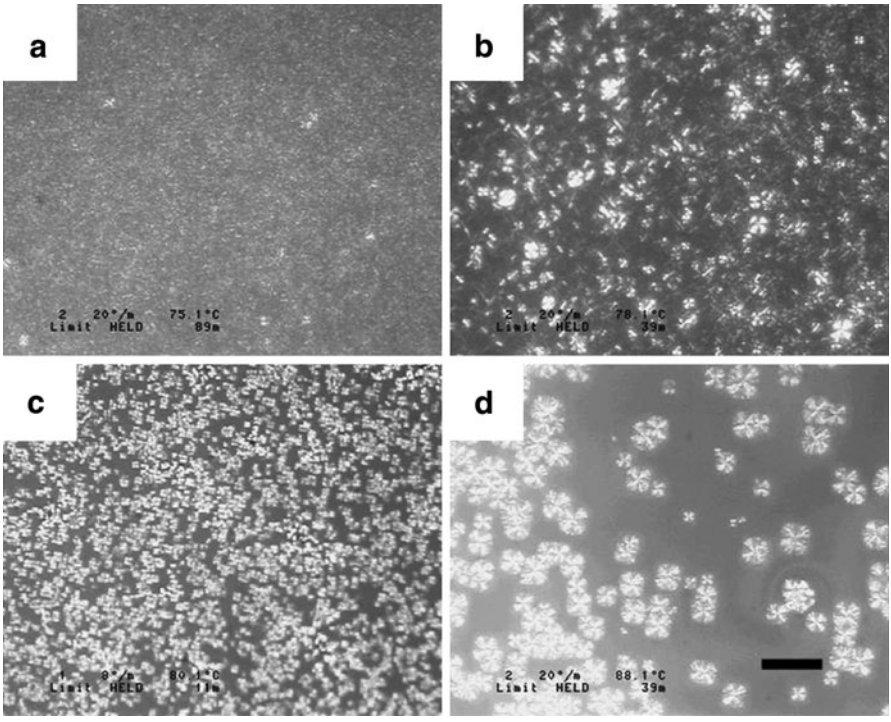

Fig. 5 Morphologies in PLLA homopolymer films crystallized at **a** 75, **b** 78, **c** 80, and **d** 88 °C from melt state. The *bar* corresponds to 100 μm

that crystallization of PLLA block determined the morphologies and phase structures. However, the addition of PEO block also affects the crystallization behavior of PLLA, and the morphologies and phase structures of the copolymers.

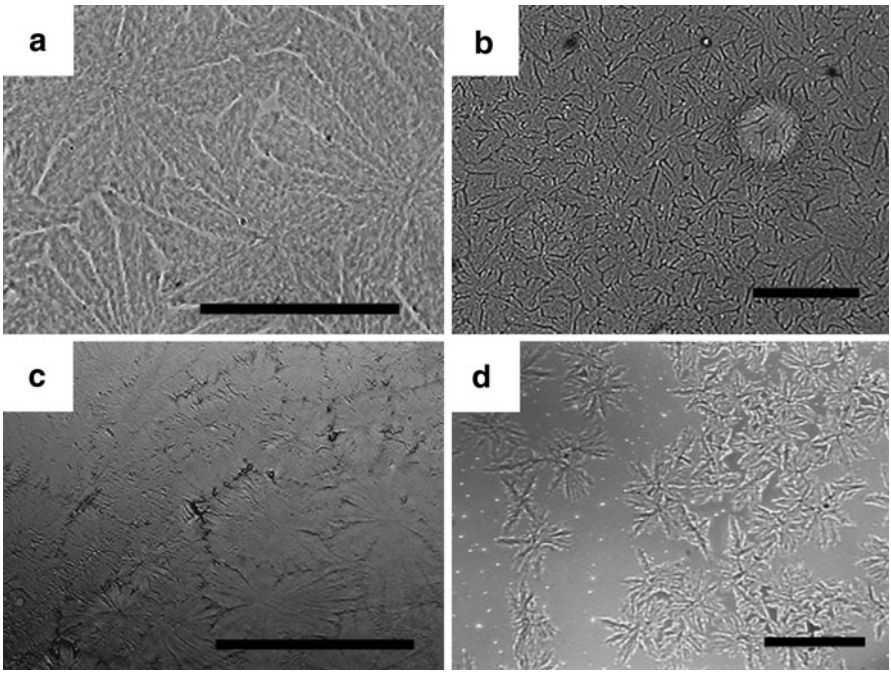

Fig. 6 Morphologies in PLLA16k-*b*-PEO5k copolymer films crystallized at **a** 110, **b** 115, **c** 120, and **d** 125 °C from 30 °C with heating after quenching from annealing temperature. The *bar* corresponds to 100 μm

Morphologies and structures determined by crystallization, microphase separation, and vitrification in process B

A distinct annealing process (named process B) was carried out. PLLA-*b*-PEO copolymer films were completely melted, and then quickly cooled to 30 °C, which is below the T_g of PLLA block, kept at 30 °C for 5 min, and then heated to the temperatures for isothermal crystallization. During the annealing and isothermal process at 30 °C, microphase separation occurs driven by crystallization of PEO component in PLLA16k-*b*-PEO5k copolymer [15, 16, 19], and even maybe immiscibility of the two unlike blocks.

When heated above T_g of PLLA block and T_m of PEO block, PEO blocks melts, and PLLA chain segments start to move. However, PLLA-*b*-PEO copolymers are not homogeneous at low temperature. Consequently, the crystallization of PLLA block in process B is from ordered state, which is absolutely different from that in process A.

Morphologies of the diblock copolymers prepared at various T_c in process B are shown in Fig. 6 for PLLA16k-*b*-PEO5k films and Fig. 7 for PLLA30k-*b*-PEO5k films. Star-shaped (or flower-shaped) morphologies were observed in the films shown. No Maltese cross can be seen by POM, and the boundary lines of the two morphologies are not linear but irregularly curvilinear, which both confirm that the

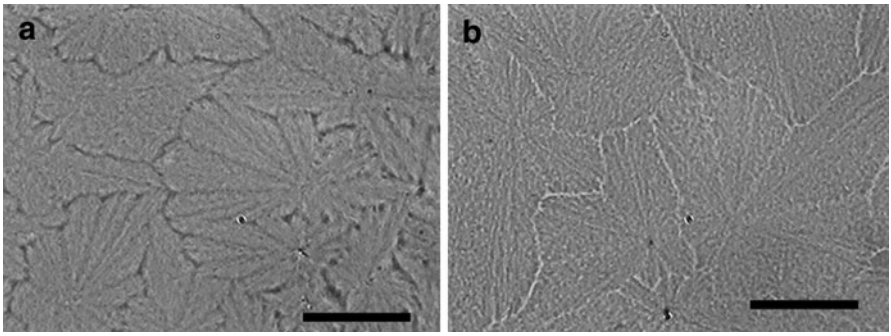

Fig. 7 Morphologies in PLLA30k-*b*-PEO5k copolymer films crystallized at **a** 110 and **b** 120 °C from 30 °C with heating after quenching from annealing temperature

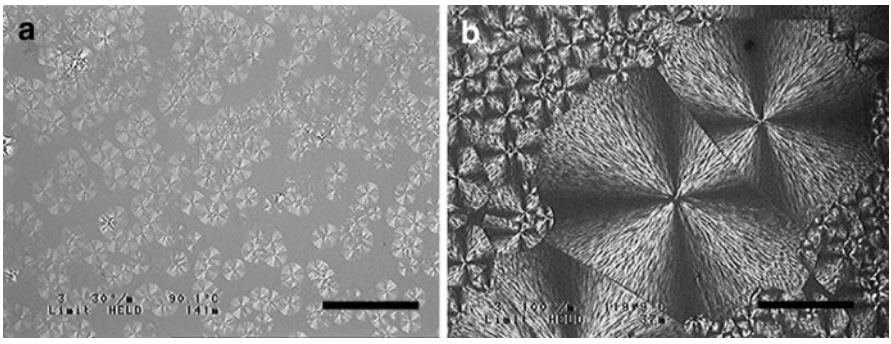

Fig. 8 Morphologies of PLLA homopolymer films crystallized at **a** 90 and **b** 120 °C heated from 30 °C after quenched from melt state. The *bar* corresponds to 100 μm

morphologies are not spherulites, but a new kind of morphologies which has never been reported for PLLA and its copolymers. In comparison, the crystalline morphologies of PLLA homopolymer crystallized at the same condition as process B are shown in Fig. 8, and they are spherulites at crystallization temperatures of 90 and 120 °C. The differences of the morphologies shown in Figs. 2, 6, 7, and 8 indicate the pre-structure formed during annealed process greatly affect the crystallization and morphology.

In order to get more information of the star-shaped morphology, AFM was used, and their typical height and the phase images are shown in Fig. 9. It is found that the morphological features are absolutely different from those of PLLA-*b*-PEO copolymers in melt crystallization and PLLA homopolymer. The morphologies shown in Figs. 6 and 7, which are tens microns or even a hundred microns in size, are composed of lozenge-shaped and truncated lozenge-shaped PLLA crystals shown in Fig. 9. The thickness of the lamellae is nanometer scale, which is same as that of PLLA single crystal. Multi-layer structure can be observed in Fig. 9a–a′, b–b′, and

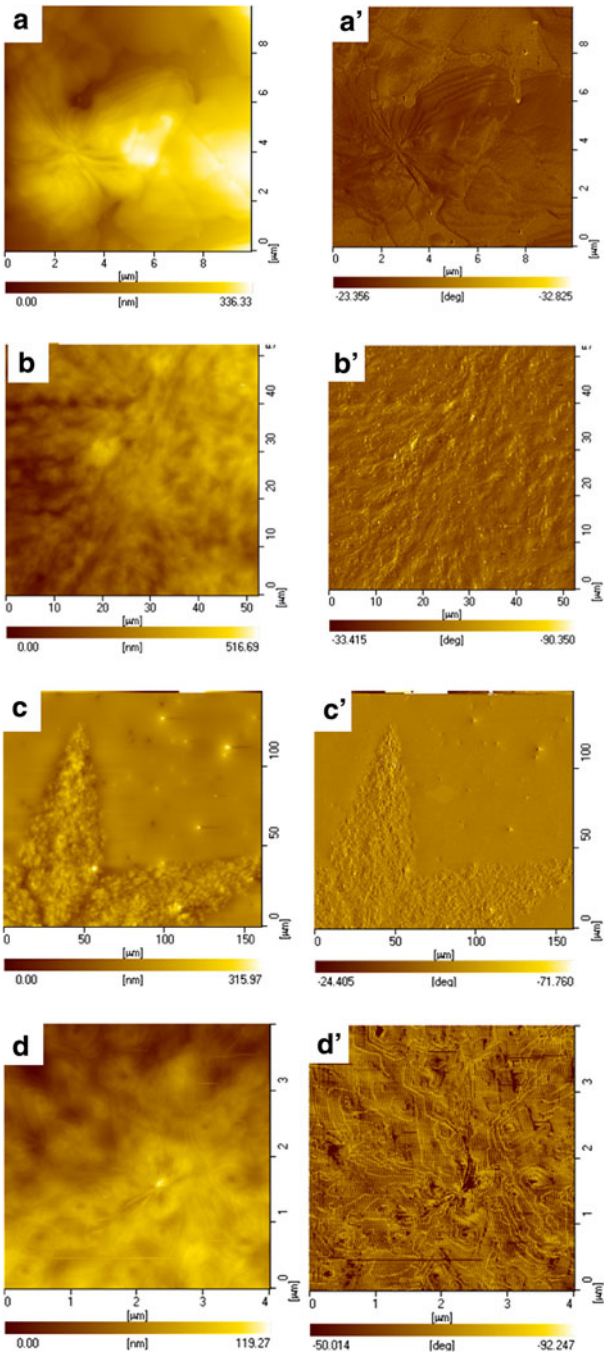

Fig. 9 AFM images of PLLA-*b*-PEO copolymer films. PLLA16k-*b*-PEO5k: crystallized at **a** 130, **b** 110, and **c** 125 °C; PLLA30k-*b*-PEO5k: **d** 110 °C from 30 °C with heating after quenching from annealing temperature

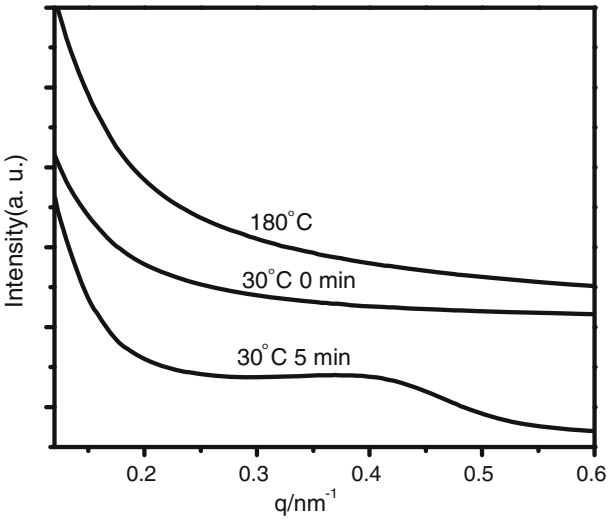

Fig. 10 SAXS profiles of PLLA16k-*b*-PEO5k diblock copolymer obtained at 180 °C and quenched from 180 to 30 °C at 0 and 5 min

c–c′, and lamellae with abundance of screw dislocation are shown in Fig. 9d–d′. Meanwhile, Fig. 9b–b′ and c–c′ indicate that the superstructure shown in Fig. 6 is stacked with small crystals. Morphologies stacked with lozenge-shaped crystals of PLLA have been reported in PLLA homopolymer thin films and PLLA diblock copolymer thin films in melt crystallization [15, 16, 19, 20]. Lozenge-shaped and truncated lozenge-shaped PLLA crystals formed in PLLA-*b*-PEO thick films (shown in Fig. 9a–a′ and d–d′) in process B indicate that the amorphous layer is sandwiched between the PLLA-rich layers, and the average PLLA-rich layer thickness is much smaller than the copolymer film thickness.

The copolymers were disordered when melted at 180 °C shown by the SAXS profile labeled 180 °C in Fig. 10. PLLA blocks do not crystallize during the annealing process because of the rapid cooling rate. When temperature is below T_g of PLLA block, vitrification of PLLA-rich phase may occur. Because of the rapid cooling rate, vitrification of PLLA chains is probably lagged to the temperature. As a result, there is no peak in the SAXS profile labeled 30 °C 0 min in Fig. 10. When temperature reaches T_c of PEO block in PLLA16k-*b*-PEO5k copolymer, PEO can crystallize [16]. Consequently, there is a peak in SAXS profile at 30 °C, isothermal for 5 min shown in Fig. 10, indicating the occurrence of phase structure transition driven by crystallization of PEO block and vitrification of PLLA block. Alternate PLLA- and PEO-rich domain can be formed.

The initial stage of crystallization process of the PLLA16k-*b*-PEO5k copolymers at 120 °C in process B was followed by SAXS, and the results are shown in Fig. 11a. In process B, the crystallization of PLLA is heating from 30 °C (below T_g of PLLA block), while in melt crystallization, the crystallization of PLA is annealed from complete melt. Obviously, the mobility of PLLA chain segments in process B

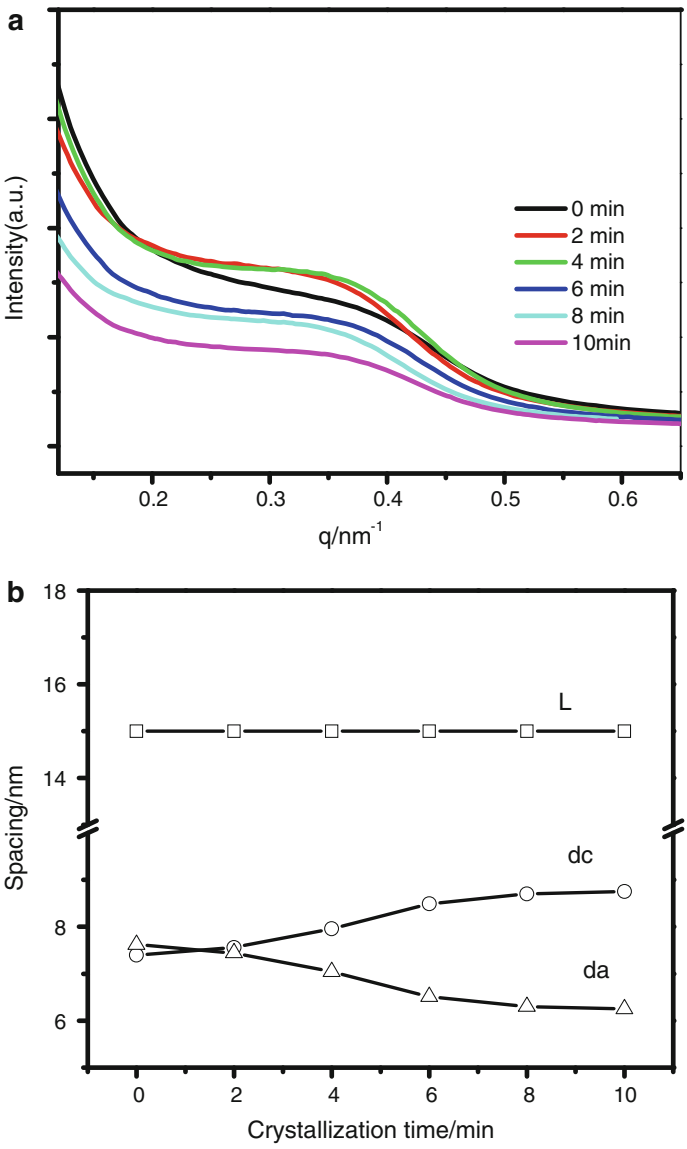

Fig. 11 **a** SAXS profiles of PLLA16k-*b*-PEO5k copolymer isothermally crystallized at 120 °C for 0, 2, 4, 6, 8, 10 min from 30 °C with heating after annealing from 180 °C. **b** Structure transition during the crystallization process

is relatively weaker, and the confinement of microstructure on PLLA chain diffusion is relatively larger, so the crystallization growth rate is smaller than that in melt crystallization.

The structural parameters including the long period (L), crystal thickness (d_c), and amorphous layer thickness (d_a) as a function of crystallization time are shown in Fig. 11b. The long period exhibits a nearly constant value from 0 to 10 min and the

crystal thickness increases with time, while the amorphous layer thickness decreases with time. The changes of the structural parameters in Fig. 11b indicate that the crystallization of PLLA block may occur within the PLLA-rich microdomains in the initial stage. The amorphous phase confines the diffusion and crystallization growth of PLLA block. Dendrites can be consequently formed as shown in Figs. 6 and 7. The size of these PLLA-rich domains is much smaller than the film thickness, which may be hundreds nanometers or even tens nanometers. In such a small domain, lozenge-shaped and truncated lozenge-shaped crystals can be formed [15–18, 33–38].

Conclusions

The morphological features and phase structure of PLLA16k-*b*-PEO5k and PLLA30k-*b*-PEO5k crystalline–crystalline diblock copolymers determined by crystallization of PLLA or PEO blocks, microphase separation of the copolymers and vitrification of PLLA block were investigated by POM, AFM, and synchrotron SAXS. In melt crystallization, microphase separation of the copolymers is driven by the crystallization of PLLA block, and microstructures formed by simultaneous microphase separation has soft confinement on further crystallization of PLLA block. The crystallization of PLLA will cover the pre-structure, and determine the final morphology. Morphological transition from spherulite to various dendritic morphologies with T_c is observed, which is probably related with the increase of the volume fraction of amorphous phase.

The phase structure transition in process B is complicated. In PLLA16k-*b*-PEO5k copolymer thick films, microphase separation is driven by crystallization of PEO block (or even immiscibility of PLLA and PEO blocks at low temperature). The pre-structure formed by microphase separation and vitrification of PLLA block will affect the crystallization and morphology of the copolymers. Star-shaped morphologies stacked with PLLA single crystals were observed. The amorphous layer divides the PLLA-rich phase into small domains, which is much smaller than the copolymer film thickness. As a result, lozenge-shaped and truncated lozenge-shaped PLLA crystals can be formed.

Acknowledgments This work is supported by the National Natural Science Foundation of China (50773082, 20974077, 51073157) and subsidized by the Special Funds for National Basic Research Program of China (2010CB631102). We appreciate the assistance of Prof. Zhonghua Wu, High Energy Accelerator Research Organization, Beijing, Chinese Academy of Sciences.

References

1. Castillo RV, Müller AJ (2009) Crystallization and morphology of biodegradable or biostable single and double crystalline block copolymers. Prog Polym Sci 34:516–560
2. Kathryn EU, Scott MC, Robert SL, Kevin MS (1999) Polymeric systems for controlled drug release. Chem Rev 99:3181–3198
3. Bates FS, Fredrickson GH (1990) Block copolymer thermodynamics-theory and experiment. Annu Rev Phys Chem 41:525–557

4. Hamley IW (1999) Crystallization in block copolymers. Adv Polym Sci 148:113–137
5. Nandan B, Hsu JY, Chen HL (2006) Crystallization behavior of crystalline-amorphous diblock copolymers consisting of a rubbery amorphous block. Polym Rev 46:143–172
6. Zhu L, Chen Y, Zhang A, Calhoun BH, Chun M, Quirk R, Cheng S, Hsiao B, Yeh F, Hashimoto T (1999) Phase structures and morphologies determined by competitions among self-organization, crystallization, and vitrification in a disordered poly(ethylene oxide)-b-polystyrene diblock copolymer. Phys Rev B 60(14):10022–10030
7. Zhu L, Cheng SZD, Calhoun BH, Ge Q, Quirk RP, Thomas EL, Hsiao B, Yeh F, Lotz B (2000) Crystallization temperature-dependent crystal orientations within nanoscale confined lamellae of a self-assembled crystalline-amorphous diblock copolymer. J Am Chem Soc 122:5957–5967
8. Muller AJ, Arnal ML, Balsamo V (2007) Crystallization in block copolymers with more than one crystallizable block. Lect Notes Phys 714:229–259
9. Rangarajan P, Register RA, Adamson DH, Fetters LJ, Bras W, Naylor S, Ryan AJ (1995) Dynamics of structure formation in crystallizable block copolymers. Macromolecules 28:1422–1428
10. Nojima S, Kato K, Yamanoto S, Ashida T (1992) Crystallization of block copolymers. 1. Small-angle X-ray scattering study of an epsilon-caprolactone butadiene diblock copolymer. Macromolecules 25:2237–2242
11. Reiter G, Castelein G, Sommer JU, Röttele A, Thurn-Albrecht T (2001) Direct visualization of random crystallization and melting in arrays of nanometer-size polymer crystals. Phys Rev Lett 87:226101–226104
12. Hamley IW, Castelletto V, Castillo RV, Müller AJ, Martin CM (2005) Crystallization in poly(L-lactide)-b-poly(epsilon-caprolactone) double crystalline diblock copolymers: a study using X-ray scattering, differential scanning calorimetry, and polarized optical microscopy. Macromolecules 38:463–472
13. Ryan AJ, Hamley LW, Bates FS (1995) Structure development in semicrystalline diblock copolymers crystallizing from the ordered melt. Macromolecules 28:3860–3868
14. Rangarajan P, Register RA, Fetters LJ, Bras W, Naylor S, Ryan AJ (1995) Crystallization of a weakly segregated polyolefin diblock copolymer. Macromolecules 28:4932–4938
15. Sun JR, Hong ZK, Yang LX, Tang ZH, Chen XS, Jing XB (2004) Study on crystalline morphology of poly(L-lactide)-poly(ethylene glycol) diblock copolymer. Polymer 45:5969–5977
16. Huang SY, Jiang SC, An LJ, Chen XS (2008) Crystallization and morphology of poly(ethylene oxide-b-lactide) crystalline-crystalline diblock copolymers. J Polym Sci B 46:1400–1411
17. Södegard A, Stolt M (2002) Properties of lactic acid based polymers and their correlation with composition. Prog Polym Sci 27:1123–1163
18. Nojima S, Toei M, Hara S, Tanimoto S, Sasaki S (2002) Size dependence of crystallization within spherical microdomain structures. Polymer 43:4087–4090
19. Yang JL, Zhao T, Zhou YC, Liu LJ, Li G, Zhou EL, Chen XC (2007) Single crystals of the poly(L-lactide) block and the poly(ethylene glycol) block in poly(L-lactide)-poly(ethylene glycol) diblock copolymer. Macromolecules 40:2791–2797
20. Huang SY, Jiang SC, An LJ, Chen XS (2009) Dendritic superstructures and structure transitions of asymmetric poly(L-lactide-b-ethylene oxide) diblock copolymer thin films. Langmuir 25(22): 13125–13132
21. Shin D, Shin K, Aamer KA, Tew GN, Russell TP, Lee JH, Jho JY (2005) A morphological study of a semicrystalline poly(L-lactic acid-b-ethylene oxide-b-L-lactic acid) triblock copolymer. Macromolecules 38:104–109
22. Fujiwara T, Miyamoto M, Kimura Y (2000) Crystallization-induced morphological changes of a poly(L-lactide)/poly(oxyethylene) diblock copolymer from sphere to band via disk: a novel macromolecular self-organization process from core-shell nanoparticles on surface. Macromolecules 33:2782–2785
23. Kim K, Chung S, Chin I, Kim M, Yoon J (1999) Crystallization behavior of biodegradable amphiphilic poly(ethylene glycol)-poly(L-lactide) block copolymers. J Appl Polym Sci 72:341–348
24. Maglio G, Migliozzi A, Palumbo R (2003) Thermal properties of di- and triblock copolymers of poly(L-lactide) with poly(oxyethylene) or poly(epsilon-caprolactone). Polymer 44:369–375
25. Li S, Vert M (2003) Synthesis, characterization, and stereocomplex-induced gelation of block copolymers prepared by ring-opening polymerization of L(D)-lactide in the presence of poly(ethylene glycol). Macromolecules 36:8008–8014
26. Hammersley A (1998) Computer program Fit2D, version V12.012, ESRF

27. Tasuniwa M, Tsubakihara S, Iura K, Ono Y, Dan Y, Takahashi K (2006) Crystallization behavior of poly(L-lactic acid). Polymer 47:7554–7563
28. Xu J, Guo B, Zhou J, Li L, Wu J, Kowalczuk M (2005) Observation of banded spherulites in pure poly(L-lactide) and its miscible blends with amorphous polymers. Polymer 46:9176–9185
29. Maillard D, Prud'homme RE (2008) Crystallization of ultrathin films of polylactides: from chain chirality to lamella curvature and twisting. Macromolecules 41:1705–1712
30. Hideto T, Yasufumi T, Swapan KS, Masakazu S, Shinichi I (2005) Spherulite growth of L-lactide copolymers: effects of tacticity and comonomers. Polymer 46:4917–4927
31. Zhang J, Tashiro K, Tsuji H, Domb AJ (2008) Disorder-to-order phase transition and multiple melting behavior of poly(L-lactide) investigated by simultaneous measurements of WAXD and DSC. Macromolecules 41:1352–1357
32. Cho TY, Strobl G (2006) Temperature dependent variations in the lamellar structure of poly(L-lactide). Polymer 47:1036–1043
33. Zhang J, Duan Y, Sato H, Tsuji H, Noda I, Yan S, Ozaki Y (2005) Crystal modifications and thermal behavior of poly(L-lactic acid) revealed by infrared spectroscopy. Macromolecules 38:8012–8021
34. Di Lorenzo ML (2001) Determination of spherulite growth rates of poly(L-lactic acid) using combined isothermal and non-isothermal procedures. Polymer 42:9441–9446
35. Abe H, Kikkawa Y, Iuoue Y, Doi Y (2001) Morphological and kinetic analyses of regime transition for poly[(S)-lactide] crystal growth. Biomacromolecules 2:1007–1014
36. Mijović J, Sy J-W (2002) Molecular dynamics during crystallization of poly(L-lactic acid) as studied by broad-band dielectric relaxation spectroscopy. Macromolecules 35:6370–6376
37. Fujita M, Doi Y (2003) Annealing and melting behavior of poly(L-lactic acid) single crystals as revealed by in situ atomic force microscopy. Biomacromolecules 4:1301–1307
38. Iwata T, Doi Y (1998) Morphology and enzymatic degradation of poly(L-lactic acid) single crystals. Macromolecules 31:2461–2467